Nanoscale

PAPER

View Article Online
View Journal | View Issue

Cite this: *Nanoscale*, 2025, **17**, 9232

Self-assemblies of cell-penetrating peptides and ferrocifens: design and biological evaluation of an innovative platform for lung cancer treatment†

Léna Guyon,‡[a] Abdallah Ladaycia,‡[a] Agnese Bosio,[a] Laurent Lemaire,[a,b] Florence Franconi,[a,b] Bénédicte Lelièvre,[c] Nolwenn Lautram,[a] Pascal Pigeon,[d,e] Gérard Jaouen,[d,e] Catherine Passirani[a] and Elise Lepeltier *[a,f]

Chemotherapy, currently used for lung cancer treatment, often consists in a combination of drugs with a moderate efficacy and severe side effects. A major drawback of the classical inorganic drugs used is their hydrophobicity, leading to a very low blood availability and weak efficacy. To overcome this constraint, a nanoplatform was set up in order to vectorize a ferrocifen drug, an organometallic tamoxifen derivative known for its really potent *in vitro* activity, but as well for its poor water solubility. Two different ferrocifens were tested: P54 and P819. The covalent conjugation of a cell-penetrating peptide (CPP) to the ferrocifen was performed, leading to an amphiphilic prodrug, potentially able to self-assemble. The CPPs used in this study are polyarginines and RLW. Moreover, in order to bring stealth and mucopenetration properties, polyethylene glycol (PEG) was incorporated into the nanostructure. The co-nanoprecipitation of CPP–ferrocifen and PEG–ferrocifen was investigated to achieve self-assemblies. A comparison of the biological activities of different suspensions was performed *in vitro* on a healthy cell line and on two different lung cancer cell lines. The biological activity of P54 was increased by a factor of 9 with the Arg_9–P54 suspension by increasing the cell internalization. Moreover, the P54-based-self-assemblies were chosen to test their *in vivo* activity on mice bearing lung tumors. The results showed that the intratracheal nebulization of Arg_9–P54/PEG–P54 or Arg_9–P54 suspensions slowed up significantly the evolution of lung cancer in mice: the suspension with PEG brought an additional comfort to the animal during the administration.

Received 13th February 2025,
Accepted 4th March 2025

DOI: 10.1039/d5nr00643k

rsc.li/nanoscale

Introduction

Lung carcinoma is the major cause of cancer-related death worldwide,[1] more particularly non-small cell lung cancers (NSCLCs), accounting for about 85% of all lung cancer diagnosis.[2] The chemotherapy treatment currently used consists in a drug combination: usually, cisplatin or carboplatin is used in combination with vinorelbine, gemcitabine, paclitaxel, docetaxel or pemetrexed.[3–5] Despite continuous improvements in treatments, the prognosis is poor, the efficacy is moderate and there are severe side effects. Thus, the development of new approaches is needed. In the last decade, numerous nanocarriers have been designed as a transport module for anticancer drugs. Among them, self-assemblies formed by peptides and more particularly by cell-penetrating peptides (CPP) have recently emerged as promising systems for controlled delivery of drugs.[6–8] In fact, peptides have attractive properties due to their simple structure, biocompatibility and chemical diversity. In addition, CPPs have the ability to cross cell membranes and enhance the intracellular delivery of conjugated cargos.[9,10] CPPs are usually short peptides, containing a high relative abundance of positively charged amino acids such as arginine and/or lysine.[11] Two main strategies for formulating drug-loaded nanostructures formed by peptides can be used. The first one is to physically encapsulate drugs into nanostructures formed of peptides. Stupp *et al.* used this strategy and synthesized amphiphilic peptides that can self-assemble into nanofibers.[12] These nanostructures were used as vectors in order to carry camptothecin.[13] The second one is used to

[a]*Univ Angers, Inserm, CNRS, MINT, SFR ICAT, F-49000 Angers, France. E-mail: elise.lepeltier@univ-angers.fr*
[b]*Univ Angers, Univ Rennes, INRAE, Inserm, CNRS, PRISM, Biogenouest, F-49000 Angers, Rennes, France*
[c]*Centre régional de pharmacovigilance, Laboratoire de pharmacologie-toxicologie, CHU Angers, 4 rue Larrey, F-49100 Angers, France*
[d]*CNRS, Institut Parisien de Chimie Moléculaire (IPCM), Sorbonne Université, 4 Place Jussieu, 75005 Paris, France*
[e]*PSL, Chimie ParisTech, 11 Rue Pierre et Marie Curie, 75005 Paris, France*
[f]*Institut Universitaire de France (IUF), France*

†Electronic supplementary information (ESI) available. See DOI: https://doi.org/10.1039/d5nr00643k

‡These authors contributed equally to this work.

covalently link peptides to drugs in order to form peptide–drug conjugates. If amphiphilic, the conjugates could potentially self-assemble into nanostructures. To this end, Cui's group has designed and synthesized a taxol–peptide conjugate that self-assembled into supramolecular filaments with a final drug loading of 41%.[14] This last strategy allows an increase of drug loading compared to the drug-encapsulated peptide nanoparticle strategy.

Over the past few years, Pr. Jaouen and his team have developed potent bioorganometallic complexes for anticancer application. Their chemistry is based on the coupling between a ferrocene moiety and a hydroxytamoxifen molecule in order to form ferrocifen molecules.[15,16] The mechanism of action is related to the redox features of Fe through reversible Fe^{II}/Fe^{III} oxidation, leading to the production of ROS species and a quinone methide, known to perform macromolecular interactions with the thioredoxin reductase system, glutathione or DNA. Interestingly, ferrocifens are able to act by causing senescence at low concentrations and apoptosis or the Fenton reaction with increasing concentrations. Moreover, ferrocifens have shown impressive *in vitro* biological activity. For instance, FcOHTam,[17] one of the first studied ferrocifens, had an IC_{50} of 0.5 μM against hormone-independent breast cancer cells,[15] highly interesting compared with those of ferrocene and hydroxytamoxifen taken separately (160 μM and 30 μM, respectively). However, ferrocifens are highly insoluble in water, requiring a formulation stage before being *in vivo* administered.

Recently, we proposed the design of an innovative platform in order to transport a hydrophobic ferrocifen (P54).[7,8] In this study, the synthesis of amphiphilic conjugates (CPP–P54) formed by two different cell-penetrating peptides Arg_n–P54 (n = 6 to 9) and RLW–P54, their self-assembly in water and the complete characterization of the nano-objects formed were performed. RLW (with a primary sequence of RLWMRWYSPRTRAYG) is known in the literature to specifically target A549 cells.[18–20] Polyarginines (Arg_n, n = 6–9), known to possess remarkable internalization properties when they have between 6 and 9 arginine units, were used for comparison as CPP models.[21] In fact, these polycationic peptides have even been found to enter cells more effectively than other homopolymers.[22] In a previous study,[7] the importance of combining several analytical methods to determine an important parameter such as the diameter of self-assemblies was underlined; indeed, it has been demonstrated that DLS was not adapted for these nanoparticles. In this work, we wanted to extend this innovative platform to another ferrocifen and to go deeper *in vitro* and *in vivo*.

In order to improve the bioavailability and efficacy of the self-assemblies, a local administration route, the intrapulmonary route *via* nebulization, has been chosen. Administering this system by nebulization would allow drug delivery close to the cancer site, and hence provide an opportunity to administer a smaller quantity of the drug for the same or a better effect while decreasing its side effects.[23,24] Also, administering chemotherapy *via* nebulization would be more tolerable by the patient than an intravenous route and would allow outpatient care.

The biological activity of the self-assemblies was assessed against two non-small cell lung cancer cell lines (A549 and NCI-H460) and against one healthy human bronchial epithelium cell line (BEAS-2B). Quantification of the internalization was evaluated in order to characterize the potential specificity of CPPs. Moreover, the addition of polyethylene glycol (PEG) into a selected CPP–ferrocifen nanostructure was investigated *in vitro* and *in vivo*. Indeed, PEG will bring stealth and CPP protection to the formulated nanosystem.[25–28] For this, PEG–ferrocifen conjugates were synthesized and the co-nanoprecipitation of CPP–ferrocifen and PEG–ferrocifen was investigated using a solvent displacement technique at different molar ratios of CPP–ferrocifen *versus* PEG–ferrocifen. *In vitro* studies were performed on healthy A549 and NCI-H460 cell lines. Finally, *in vivo* experiments were carried out on an orthotopic NCI-H460 tumor immunodepressed murine model,[29] the intratracheal administration route[30–32] allowing the suspension to be sprayed directly into the lung and resulting in deposition in the smaller airways (bronchi and bronchioles).

Results and discussion

Synthesis and characterization of conjugates

From the different ferrocifen derivatives, two were chosen: P54[7] and P819.[33] P54 was chosen thanks to its carboxylic acid group that would facilitate different coming chemical reactions. On the other hand, P819, in addition to the presence of the carboxylic group, allowing to perform chemical reactions similar to those applied on P54, has the advantage to generate, once metabolized by the organism, a metabolite that has been shown to have a better *in vitro* cytotoxicity than P54[34] (Fig. 1).

In order to formulate ferrocifen-based self-assemblies with the aim of improving ferrocifen solubility and bioavailability, two kinds of amphiphilic compounds were synthesized. First, Arg_9–ferrocifen conjugates. Arg_9 was covalently linked to the ferrocifen moiety through an amide bond at the end of the solid phase peptide synthesis; this synthesis has been described previously.[7] This coupling was performed for both ferrocifens and so gave two different conjugates: Arg_9–P54 and Arg_9–P819. These conjugates would help improving the solubi-

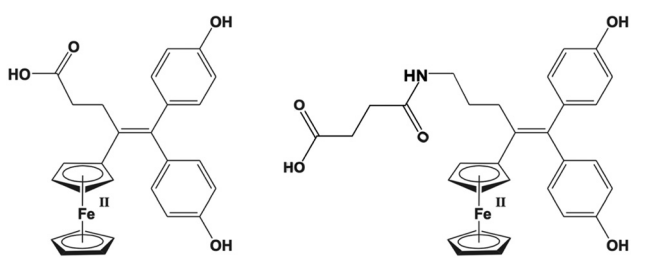

Fig. 1 Molecular structures of P54 (on the left) and P819 (on the right).

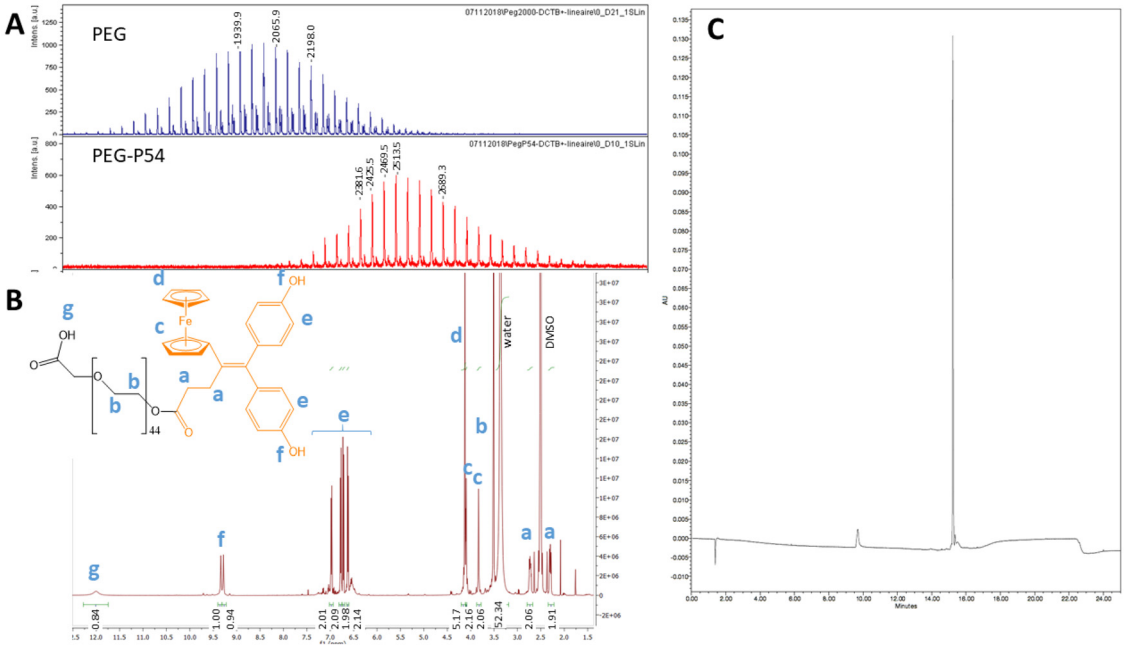

Fig. 2 Characterization of purified PEG–P54: (A) MALDI-TOF spectra of free PEG and PEG–P54 in linear mode, (B) ^{1}H NMR spectrum in deuterated dimethyl sulfoxide and (C) UPLC chromatogram of PEG–P54 at 450 nm.

lity and cell internalization of ferrocifen. The second type of conjugate was synthesized by linking PEG_{2000} to ferrocifen *via* an ester bond using HBTU as a coupling reagent; two PEG-based conjugates were synthesized, PEG–P54 and PEG–P819. The objective was to overcome the different biological barriers existing with a pulmonary administration route such as ciliated cells, mucus and macrophages.

The different desired conjugates were successfully synthesized. After purification by RP–HPLC, Arg_9–ferrocifens were characterized by mass spectroscopy and ^{1}H NMR (ESI Fig. S1–S4†); Arg_9–P54 was obtained with a yield of 24% and a purity of 94% and Arg_9–P819 was obtained with a yield of 25% and a purity of 91%.

The PEG–ferrocifen conjugates were analyzed by ^{1}H NMR and mass spectrometry (Fig. 2A and B). The MALDI-TOF spectrum of free PEG was compared to that of PEG–ferrocifen. A shift of the PEG signal peaks (M_{P54} = 468.32 g mol^{-1} and M_{P819} = 569.47 g mol^{-1}) confirmed that the coupling reaction was successful (Fig. 2A for PEG–P54 and Fig. S10 in the ESI† for PEG–P819). PEG–P54 was obtained with a yield of around 11% and a purity of 90% (Fig. 2C) and PEG–P819 with a yield of 12% and a purity of 91%.

Once synthesized and purified, the next step was to study the potential formulation of self-assemblies using these amphiphilic conjugates; the critical aggregation concentration (CAC) was determined using the pyrene fluorescence 1 : 3 ratio method.[35] The CAC was determined from the crossover of linear fits across the different fluorescence regimes. For Arg_9–P819 self-assemblies, a CAC of 34 μM was observed (Fig. 3). Self-assemblies of Arg_9–P54 were already formulated in a previous study[7] and a CAC of 79 μM was obtained.

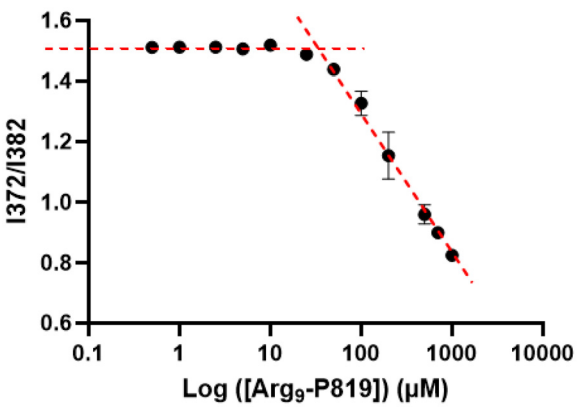

Fig. 3 Quotient of vibrational band intensities (I_1/I_3) as a function of log [Arg_9–P819].

PEG–ferrocifen being amphiphilic, its propensity to self-assemble was also investigated using the pyrene fluorescence 1 : 3 ratio method.[35] Thus, the critical aggregation concentration (CAC) of PEG–P54 was determined and compared with those previously obtained from different CPP–P54 conjugates[7] (Table 1). The CAC value obtained for PEG–P54 (243 μM) was between those of Arg_9–P54 (113 μM) and RLW–P54 (314 μM). These results were in agreement with previous studies;[36] an increase of the CAC was observed with an increase of the hydrophilic part. On the other hand, the conjugate of PEG–P819 failed to formulate stable self-assemblies. When preparing a suspension of this conjugate, the highest concentrations caused precipitation of the conjugate and the other points,

Table 1 Comparison of the different CACs obtained using the pyrene fluorescence 1 : 3 ratio method.[35] The different values obtained for CPP–P54 were determined from a previous study.[7] Quotients of vibrational band intensities (I_1/I_3) *vs.* log[conc.] for all compounds are shown in Fig. S8†

Compound	CAC (μg mL^{-1})	CAC (μM)
Arg_6–P54[7]	35	25
Arg_7–P54[7]	63	40
Arg_8–P54[7]	113	66
Arg_9–P54[7]	147	79
PEG–P54[7]	571	251
RLW–P54[7]	977	398
P54[7]	295	631
Arg_9–P819	18	34

corresponding to lower concentrations, did not form a sigmoid when fitted with the Boltzmann sigmoid.

According to these results, the formulation process by nanoprecipitation was performed at a concentration above all these CAC values. Cryo-TEM analysis was performed to observe the self-assembly morphology in its native form. According to the results obtained (Fig. S9†), the conjugates showed self-assembly into spherical particles (the presence of very small spherical objects were also observed, particularly in Fig. S9A†).

In order to determine the self-assembly diameter, the formulations were analyzed by ^{1}H NMR diffusometry (DOSY); in a previous study,[7] it has been demonstrated that DLS was not suitable to characterize these self-assemblies, in contrast to DOSY.

The principle of DOSY is that smaller self-assemblies should diffuse faster compared to larger nanostructures and should give the major contribution in terms of protons. Using DOSY 2D NMR (or pulse-field gradient-based sequence), species contributing to the signal can be separated based on both the spectral and diffusion dimensions.[37] The spectral dimension provides information on the chemical specificity to elucidate species present in the formulation. The diffusion dimension is indicative of the size of objects present in the formulation, the bigger the object, the slower the diffusion. If several objects are present, several diffusion coefficients are observed. The contribution determination of each compartment reflects the NMR visibility of each population. So, the nucleus part of a large object has often shorter transversal relaxation times and it is less NMR visible and often underestimated compared to small molecules. The DOSY results in D_2O (Fig. 4) revealed nanoparticles with an apparent diameter of 4.1 nm for Arg_9–P54, 4.5 nm for Arg_9–P819 and 4.1 nm for PEG–P54 self-assemblies (Fig. S11†).

To investigate further, we decided to focus on P54 for formulation reasons (PEG–P819 failed to form stable self-assemblies). The biological activity of Arg_n–P54 (n = 6–9) self-assemblies obtained by nanoprecipitation was assessed on three different cell lines: a healthy human bronchial epithelium cell line (BEAS-2B) and two human lung cancer cell lines (A549 and NCI-H460).

First of all, the influence of the peptide length on the cytotoxic activity was investigated in a human bronchial epithelium cell line (BEAS-2B) and the results were compared with those of free P54. The cell viability assay performed using an MTT assay after 24 hours of treatment with various concentrations showed no significant difference between the CPP–P54 suspensions and free P54: Table 2. All the IC_{50} values were in the same range and no tendency was observed in the function of the peptide length.

The same experiments were then performed on two different non-small-cell lung cancer cell lines: A549, an adenocarcinoma human alveolar basal epithelial cell line and NCI-H460, a large-cell carcinoma line. The viability assay performed on A549 showed that the peptide length had an impact on the cytotoxicity; an increase of the peptide length resulted in an increased toxicity. In fact, Arg_9–P54 was more efficient than the other suspensions. However, no statistically significant difference was observed between the suspensions and free P54. These results were confirmed on NCI-H460 cells. In fact, the same trend was observed for the peptide length efficacy; the Arg_9–P54 suspension has shown to be the most efficient (Table 2). Free P54 had a very high IC_{50}, statistically different from conjugates.

In order to overcome the polycation dilemma,[38] to protect the peptide from an early enzymatic degradation,[39] to limit the mucociliary clearance from the airways,[40] to escape macrophages[41] and to cross the mucus,[42] the idea was to incorporate PEG in the self-assembly structure. Suspensions with different molar ratios of Arg_9–P54/PEG–P54 were formulated by co-nanoprecipitation: 10/1, 2/1, 1/1 and 1/2.

Viability assays were performed on the healthy cell line (BEAS-2B cells) and on lung cancer cells (NCI-H460). On BEAS-2B cells, the same range of IC_{50} was obtained between all the different suspensions and compared to P54 alone (Table 3). The cytotoxicity of the different conjugates on the healthy cell line is globally high and all the same in the tested concentrations, probably because of the high sensitivity of this healthy cell line, a point already observed in the literature.[43]

On NCI-H460, the presence of PEG had a significant impact on the IC_{50} values; a higher IC_{50} was obtained with a higher amount of PEG, assuming that PEG could hide the CPP, causing a decrease of the biological activity[44–46] (Table 3). Moreover, it is known that PEG decreases cell uptake because of its hydrophilic nature.[47,48] In fact, PEG could shield the cell-penetrating peptide feature of Arg_9–P54, resulting in a decrease of cell internalization. It is important to note that no toxicity was observed for PEG–P54 alone in the range of tested concentrations and the highest IC_{50} was obtained for the suspension containing the highest amount of PEG (Arg_9–P54/PEG–P54: 1/2). Moreover, all the results obtained for the Arg_9–P54/PEG–P54 suspensions were statistically significant compared to those of free P54. According to these results, the 10/1 ratio was chosen for the next experiments.

This molar ratio was used to formulate self-assemblies by co-nanoprecipitation of Arg_9–P819/PEG–P819. They were characterized by DOSY in D_2O and apparent diameters of 2.9 nm for Arg_9–P54/PEG–P54 self-assemblies (Fig. 5) and 4.4 nm for Arg_9–P819/PEG–P819 were obtained (Fig. S12†).

Lung cancer was induced in nude mice by injection of lung cancer cells (NCI-H460) in the left lung of nude

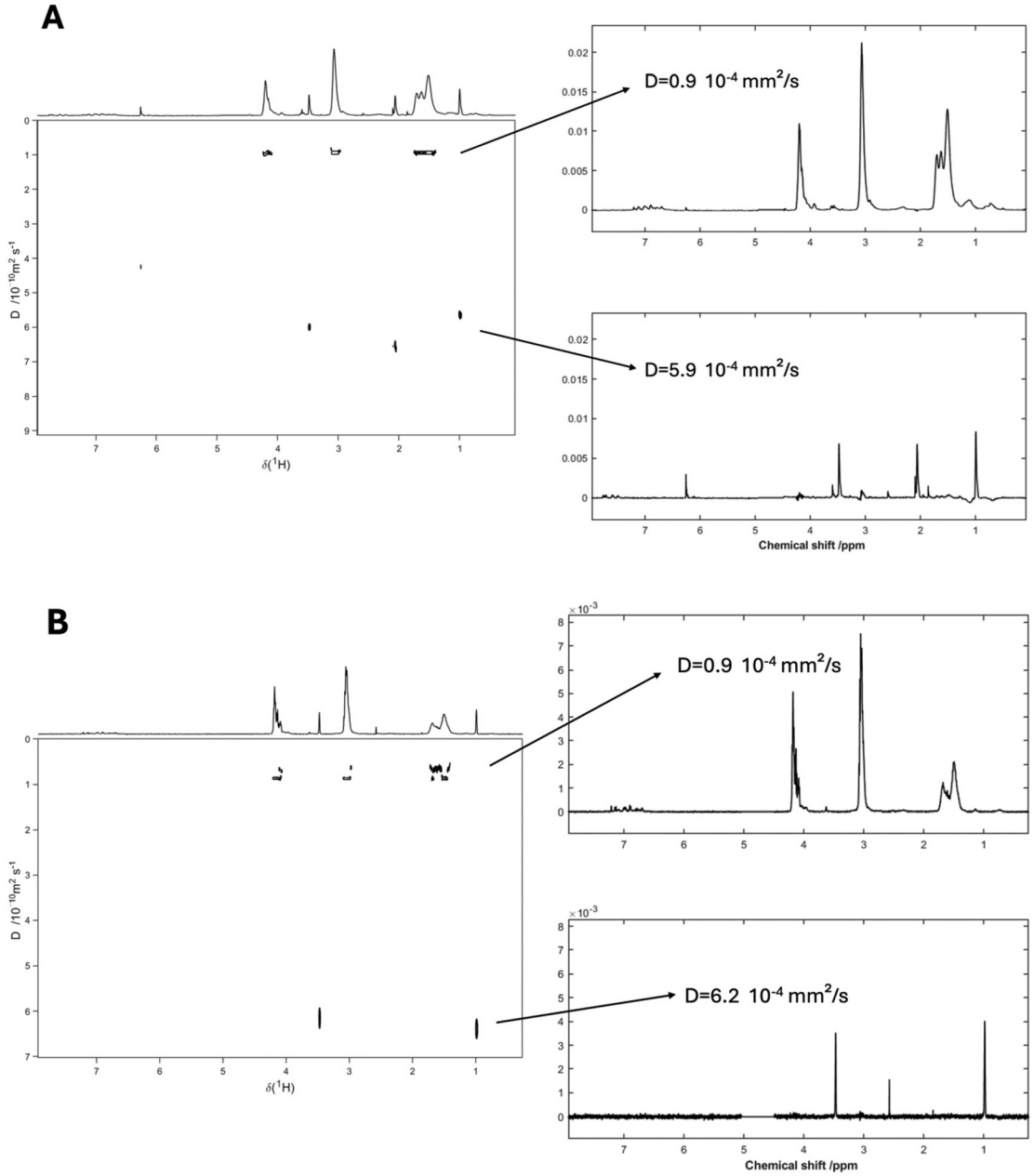

Fig. 4 (A) DOSY ^{1}H spectrum (left) of Arg_9–P54 suspension in deuterated water at 25 °C after filtration through a 0.2 μm filter and the corresponding two-component SCORE analysis (right) and (B) DOSY ^{1}H spectrum (left) of Arg_9–P819 suspension in deuterated water at 25 °C after filtration through a 0.2 μm filter and the corresponding two-component SCORE analysis (right).

mice.[29] The presence of the tumor was confirmed by MRI (Fig. S13†). First, self-assemblies of PEG–P54 were studied to evaluate their biological effect compared to the control group nebulized with phosphate-buffered saline (PBS). The administration of self-assemblies of PEG–P54 was performed by nebulization *via* an intratracheal administration using a high pressure syringe at day 9 and 12 after the cancer cell injection at a concentration of 0.24 mM in ferrocifen P54.

In order to study the tolerance in mice, their weight was measured during the whole experiment (Fig. 6A). The mice

Table 2 Biological activities of Arg_n–P54 suspensions on three cell lines obtained by an MTT assay after 24 h of treatment, expressed as a function of P54 concentration

	BEAS-2B healthy cell line		A549 cancer cell line		NCI-H460 cancer cell line	
	IC_{50} (μM)	SD	IC_{50} (μM)	SD	IC_{50} (μM)	SD
Arg_6–P54	35	2	231	1	46	1
Arg_7–P54	21	1	136	1	31	1
Arg_8–P54	12	1	111	1	31	1
Arg_9–P54	26	2	83	1	24	1
P54	27	1	216	1	215	1

Table 3 Biological activities of Arg_9–P54/PEG–P54 suspensions on two cell lines obtained by an MTT assay after 24 h of treatment

	BEAS-2B healthy cell line		NCI-H460 cancer cell line	
	IC_{50} (μM)	SD	IC_{50} (μM)	SD
Arg_9–P54/PEG–P54 10/1	19	1	34	1
Arg_9–P54/PEG–P54 2/1	20	1	53	1
Arg_9–P54/PEG–P54 1/1	25	1	77	1
Arg_9–P54/PEG–P54 1/2	25	1	105	2
PEG–P54	31	1	—	—
Arg_9–P54	26	2	24	1
P54	27	1	215	1

showed no significant loss of weight, proving a good tolerance to treatment. The tumor evolution for each group (control and treated mice) was performed using MRI. The doubling time, the time it takes for the tumor to double in volume, was then calculated for each mouse from the different groups. The results are presented in Fig. 6B.

The obtained results showed no significant effect of treatment *via* nebulization of PEG–P54 self-assemblies compared to the control group. One explanation of these results could be that the PEG chains, even if they help in overcoming the different pulmonary biological barriers, would prevent the internalization of P54 in cancer cells, limiting its anticancer efficacy.[48,49]

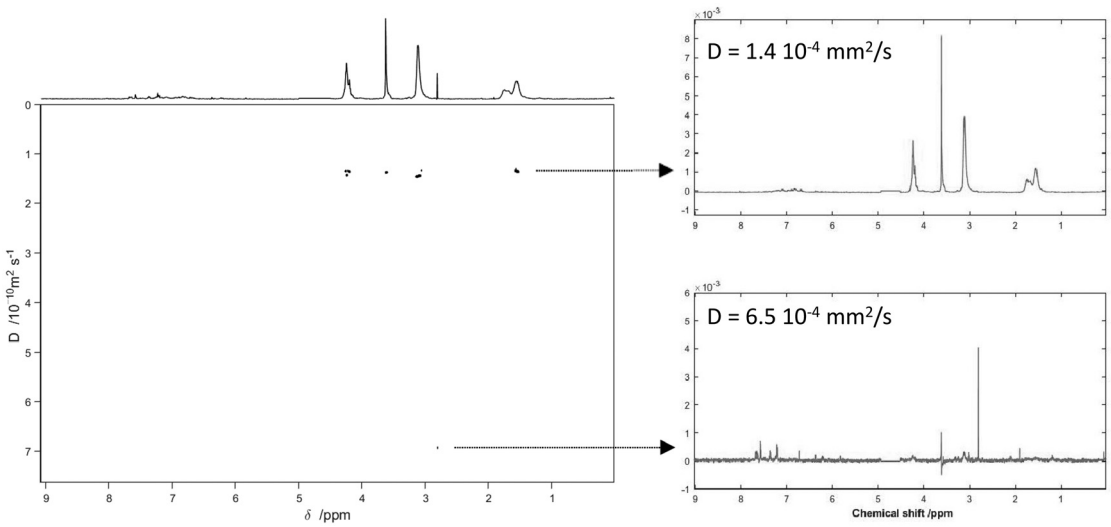

Fig. 5 DOSY ^{1}H spectrum (left) of Arg_9–P54/PEG–P54 10/1 suspension in deuterated water at 25 °C after filtration through a 0.2 μm filter and the corresponding two-component SCORE analysis (right).

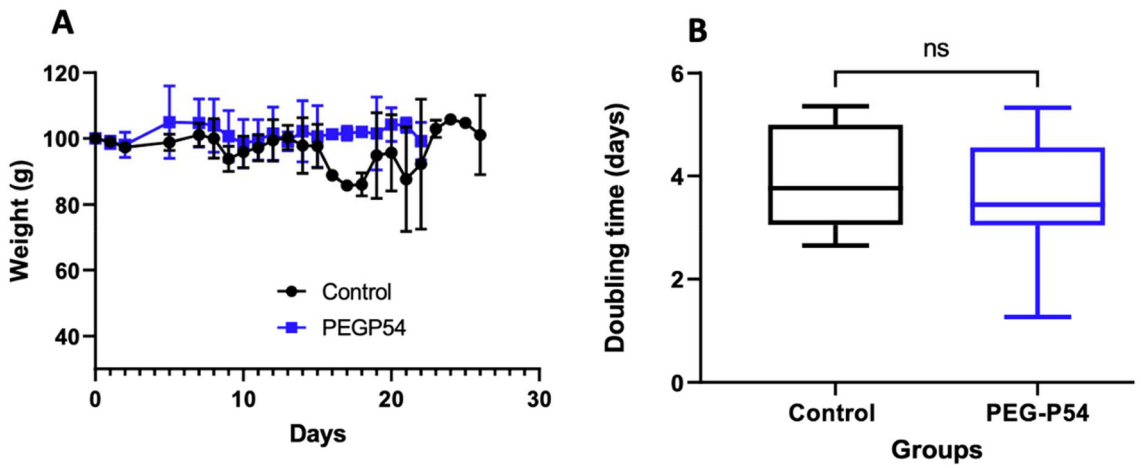

Fig. 6 (A) Mouse body weight evolution over 27 days. Control group: n = 13. PEG–P54: n = 7. (B) Tumor doubling time of the group treated with PEG–P54 self-assemblies compared to the control group nebulized by PBS. Control group: n = 13. PEG–P54: n = 7. P > 0.5. ANOVA and Student's t test were used.

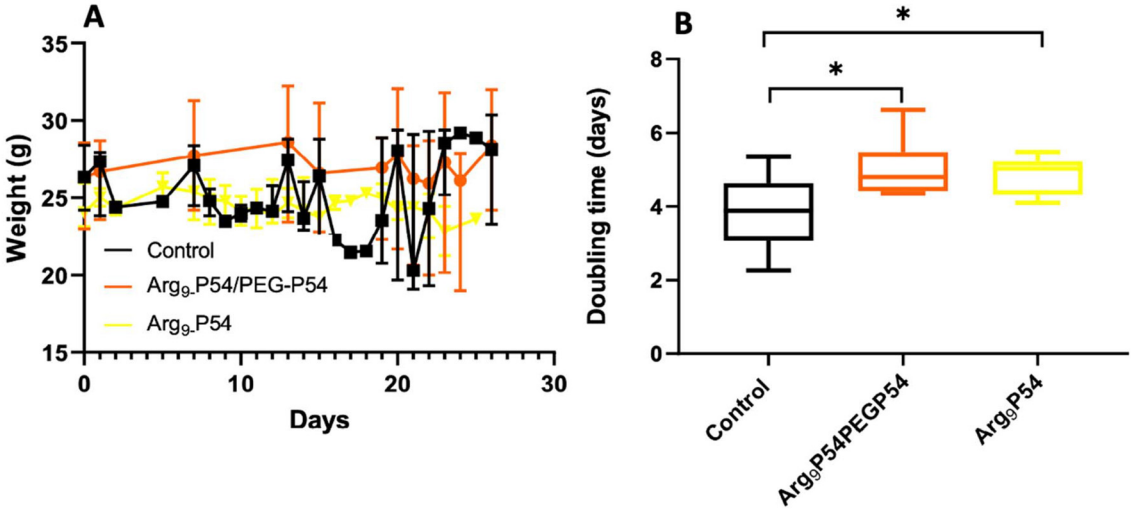

Fig. 7 (A) Mouse body weight evolution over 27 days. Control group: n = 13. Arg_9–P54/PEG–P54: n = 7, Arg_9–P54: n = 7. (B) Tumor doubling time of different groups: group treated with self-assemblies of Arg_9–P54/PEG–P54 and Arg_9–P54 compared to the control group nebulized by PBS. Control group: n = 13. Arg_9–P54/PEG–P54: n = 7, Arg_9–P54: n = 7. ANOVA followed by Dunnet's test were used.

Two self-assemblies were then studied: Arg_9–P54 and Arg_9–P54/PEG–P54 self-assemblies. Following the same protocol, the biological efficacy was evaluated *in vivo*.

First, no significant weight loss was observed (Fig. 7A); it has to be mentioned that the group treated with self-assemblies of Arg_9–P54 showed suffering signs in the first minutes after nebulization. This observation could be explained by the cell penetrating peptide Arg_9 known to show an acute toxicity after its administration because of its cationic charge causing mast cell degranulation.[50]

Nebulization was performed at day 9 and day 12 after the injection of cancer cells at a concentration of 0.24 mM in P54. The evolution of the tumor size was performed using MRI and the biological efficacy was assessed by calculating the tumor volume doubling time by fitting the growth curves with an exponential function, the time constant of the exponential being defined as the doubling time value[51] (Fig. 7B).

The results showed that compared to the control group, the treatments with nebulization of Arg_9-P54/PEG-P54 self-assemblies or Arg_9–P54 self-assemblies increased significantly ($p < 0.05$) the doubling time and so slowed down the tumor development.

To conclude, in order to combine a significant anticancer effect and a good tolerance of treatment by the mice, the self-assemblies composed of Arg_9–P54/PEG–P54 could be really promising on lung cancer treatment using a nebulization administration route.

Conclusion

In this work, it has been described for the first time that the co-nanoprecipitation of Arg_9–ferrocifen with PEG–ferrocifen results in self-assemblies; this concept was successfully demonstrated with two different ferrocifens, P54 and P819. Furthermore, the *in vivo* study showed that treatment by nebulization of Arg_9–P54/PEG–P54 self-assemblies at a molar ratio of 10/1 slowed down significantly the volume of the lung tumor on the treated mice compared to the control group. The designed self-assemblies of this project could even be modulated in modifying the peptide sequence to provide a better cancer cell specificity and/or by extending this strategy to other conventional anticancer compounds.

Materials and methods

Materials

Polyethylene glycol (HO–PEG–COOH, M_w = 2 kDa) was purchased from Creative PEGWorks (USA). Dimethylformamide (DMF), trifluoroacetic acid (TFA) and acetonitrile (ACN) were obtained from Thermo Fisher Scientific (USA). All amino acids derivatives, hexafluorophosphate (HBTU) and diisopropylethylamine (DIEA) were purchased from Iris Biotech GmbH (Germany). Phenol was obtained from Merck KGaA (Germany). Diethyl ether, LC-MS grade water and ULC/MS grade ACN were purchased from Biosolve (France). Deionized water was obtained from a Milli-Q plus system (Merck-Millipore, Germany). Ferrocifens were provided by PSL Chimie ParisTech (France). Formic acid, acetone and pyrene were obtained from Sigma-Aldrich (France).

A549 and NCI-H460 cell lines were obtained from the American Type Culture Collection (USA). Roswell Park Memorial Institute 1640 (RPMI) medium was purchased from LGC Standards (France). BEGM™ Bronchial Epithelial Cell Growth Medium BulletKit™ containing BEBM™ Bronchial Epithelial Cell Growth Basal Medium (CC-3171) and BEGM™ Bronchial Epithelial Cell Growth Medium SingleQuots™

Supplements and Growth Factors (CC-4175) were purchased from Lonza (Switzerland). Fetal bovine serum (FBS), penicillin, streptomycin and phosphate-buffered saline (PBS) were obtained from Gibco (Fisher, France). Amphotericin B was obtained from PAA Cell Culture Company (Fisher, France). MTT (3-(4,5-dimethylthiazol-2-yl)-2,5-diphenyltetrazolium bromide), Hanks' balanced salt solution (HBSS) and dimethyl sulfoxide (DMSO) were purchased from Sigma-Aldrich (USA). Trypsin-EDTA 10× was obtained from Biowest (France).

Conjugate synthesis and characterization

Synthesis and purification. Different CPPs have been synthesized by solid phase peptide synthesis *via* the Fmoc strategy and Arg_n (n = 6–9), RLW, and the conjugates CPP–P54 and CPP–P819 were synthesized, purified and characterized according to our previous study.[7]

The ferrocifen molecule was conjugated with the PEG moiety using the same strategy as that for CPP–ferrocifen synthesis. In order to activate the carboxylic acid function, ferrocifen (P54 or P819) (5 equiv.) containing a carboxylic acid function was solubilized with HBTU (5 equiv.) in DMF. After 30 min, DIEA (10 equiv.) was added to the coupling mixture and immediately PEG in DMF (5 μM) was incorporated into the solution. The reaction was stopped after 2 h and DMF was removed using a rotary evaporator.

The obtained oil was then purified by semi-preparative reversed phase high-performance liquid chromatography (RP-HPLC) using a Waters (France) instrument. Purification was performed at room temperature using a SymmetryPrep C8 column (250 × 30 mm) with 7 μm particle size and 100 Å pore size. Eluent (A) was 0.1% TFA in water while eluent (B) contained 0.1% TFA in ACN. A gradient elution was used at a flow rate of 3 mL min^{-1} and an injection volume of 250 μL (Table 4). Peaks were detected at a wavelength of 450 nm (detection of the ferrocene part). Crude oil was solubilized in 30% (A) and 70% (B) at a concentration of 5 mg mL^{-1}. The sample was vortexed and sonicated prior to injection.

Characterization

Nuclear magnetic resonance (NMR) spectroscopy. ^1H NMR spectra were recorded in deuterated dimethyl sulfoxide at 400 MHz in FT mode using a Bruker 500 MHz AVANCE III HD spectrometer (Wissembourg, France) equilibrated at 25 °C. Spectra were analyzed using the software MestReNova®.

Mass spectrometry (MS). Matrix-assisted laser-desorption ionization time-of-flight (MALDI-TOF) spectra was recorded using a Bruker Biflex III spectrometer with a wavelength laser of 337 nm. 2-[(2*E*)-3-(4-*tert*-Butylphenyl)-2-methylprop-2-enylidene] malononitrile (DCTB) was used as a matrix. Positive ion spectra were recorded in linear mode; PEG–P54 was solubilized in dichloromethane prior to acquisition.

Ultra-performance liquid chromatography (UPLC). An UPLC-UV method was developed to quantify the purity of PEG–P54 and PEG–P819. The apparatus consisted of an UPLC Acquity H-Class Bio (Waters, France) composed of a quaternary solvent manager, a sample manager, a photo diode array detector and a column manager. The system was managed using Empower®3 software (Waters). The column used was an Acquity®UPLC BEH C18 100 × 2.1 mm, 1.7 μm (Waters). The mobile phase was composed of a mixture of 0.1% TFA in water (A) and 0.1% TFA in CAN (Table 5). The flow rate was 0.2 mL min^{-1} and the injection volume was set to 10 μL. Detection was performed at 450 nm. The purified product was dissolved in 95% (A) and 5% (B) at a concentration of 1 mg mL^{-1}.

Critical aggregation concentration (CAC). The critical aggregation concentration (CAC) was determined as reported previously using pyrene as a fluorescent probe.[7] For thus, 6 μL of pyrene stock solution in acetone (50 μM) was added into tubes. Then, acetone was evaporated under dark conditions. Different suspensions of the tested conjugate with a concentration ranging from 0.5 to 2000 μM were added into tubes and mixed overnight at 37 °C in order to have a final pyrene concentration of 1 μM. After 30 min of equilibration at room temperature, a fluorescence spectrophotometer (Fluoromax-4, Horiba, Japan) was used to measure the fluorescence intensity of pyrene at an excitation wavelength of 336 nm. The emission spectra were recorded in the range 350–500 nm. The slit opening for the excitation was set at 1 nm and 3 nm for the emission. The intensity ratios of pyrene at I_{372}/I_{382} (I_1/I_3) were plotted against the log of the concentration and the results were fitted using a Boltzmann-type sigmoid. The CAC value was determined as the first sharp decrease point.[52]

Self-assembly formulations and characterization

Formulation protocol. Co-nanoprecipitation of CPP–P54/PEG–P54 and CPP–P819/PEG–P819 was performed using a solvent displacement method.[7] Briefly, the conjugates were solubilized in an adequate organic solvent (ethanol) at

Table 4 Gradient elution of the RP-HPLC method for the purification of PEG–P54. Phase (A) contained 0.1% TFA in water and phase (B) contained 0.1% TFA in ACN

Time (minutes)	Flow (mL per minutes)	Phase A (%)	Phase B (%)
0	3	97	3
26	3	25	75
40	3	10	90
42	3	10	90
43	3	97	3
50	3	97	3

Table 5 Gradient elution of the UPLC-UV method. Phase (A) contained 0.1% TFA in water and phase (B) contained 0.1% TFA in ACN

Time (minutes)	Flow (mL per minute)	Phase A (%)	Phase B (%)
0	0.2	95	5
5	0.2	78	22
10	0.2	78	22
15	0.2	0	100
20	0.2	0	100
21	0.2	95	5
25	0.2	95	5

different molar ratios of the conjugate. This organic mixture was then added drop by drop to a volume of water (4 times the volume of the organic solvent) under agitation. The organic solvent was then evaporated *via* an argon flow under agitation.

Self-assembly characterization by Cryo-TEM analysis. Cryogenic Transmission Electron Microscopy (Cryo-TEM) experiments were performed with a Cryo-TEM (Tecnai™ G2 Sphera, FEI, USA) at the Microscopy Rennes Imaging Center (Biogenouest, Rennes). A 4 μL drop of the 10 mg mL^{-1} formulation was deposited on the surface of a carbon-coated copper grid. This grid was held under controlled conditions (humidity and temperature) by tweezers on a guillotine device. In order to remove the excess sample, a filter paper was then pressed against the liquid. Then, the gird was dropped into the liquid ethane in order to vitrify the sample. The grid was then transferred to a cryo-holder. Analyses were performed at an accelerating voltage of 200 kV under a low electron dose. Data processing was performed with ImageJ software.

Self-assembly characterization by NMR diffusometry (DOSY). ^{1}H NMR pulsed field gradient acquisition (PFG-NMR), also called diffusion ordered spectroscopy (DOSY), was performed on the self-assemblies (9 mg mL^{-1}) in deuterated water at 25 °C after filtration using a 200 nm filter. A Bruker 500 MHz AVANCE III HD spectrometer (Wissembourg, France) equipped with a 5 mm BBFO probe at the ASTRAL NMR facility from Angers University was used. In DOSY measurements, diffusion coefficients were estimated related to the chemical shift by the observation of the exponential decay of the NMR signal due to the self-diffusion behaviour taking place between the two gradients of the magnetic field. Diffusion experiments were performed using a stimulated echo sequence with longitudinal eddy current delay, ledgp2s. The diffusion time was 200 ms, the diffusion gradient duration was 2.4 ms, the gradient shape ramp was linear with 128 steps and the number of averages was 96. The gradient magnitude ranged from 5 to 95% of the maximum gradient intensity (50 G cm^{-1}). Spectra were analysed using the GNAT processing platform (**https://doi-org.proxy.insermbiblio.inist.fr/10.1002/mrc.4717**). Hydrodynamic diameters were calculated from the estimated diffusion coefficient according to the Stokes–Einstein relationship.

Biological activity of suspensions: cell viability assays

The toxicity of self-assemblies was compared to free ferrocifen P54 on human lung adenocarcinoma cells (A549), human large-cell lung carcinoma (NCI-H460) and human lung epithelial cells (BEAS-2B). A549 and NCI-H460 cells were maintained in Roswell Park Memorial Institute 1640 (RPMI) medium containing 10% fetal bovine serum (FBS) and 1% antibiotics. BEAS-2B cells were maintained in Bronchial Epithelial Cell Growth Basal Medium with all the additives as recommended by the supplier. Each cell line was maintained in a humidified incubator under an atmosphere containing 5% CO_2 at 37 °C. BEAS-2B cells were sub-cultured once a week, while A549 and NCI-H460 were sub-cultured twice a week using 0.25% trypsin in EDTA (dilution 1 : 6 in HBSS). The cell viability was determined with a colorimetric assay using the succinate dehydrogenase activity of viable cells by the reduction of the yellow-colored tetrazolium salt, 3-(4,5-dimethylth-iazol-2-yl)-2,5-diphenyl tetrazolium bromide, to a purple-colored formazan crystal (MTT assay). Briefly, the cells were plated in 96-well plates at densities of 10×10^3 cells per well (A549), 10×10^3 cells per well (NCI-H460) and 20×10^3 cells per well (BEAS-2B). After 24 h, the cells were treated for 24 h with different concentrations of the self-assemblies. Then, the cells were incubated for 3 h with MTT solution (0.5 mg mL^{-1} in RPMI or BEBM medium). The medium was removed and DMSO (100 μL per well) was added to solubilize formazan crystals. The samples were finally analyzed with absorbance detection at 580 nm on a plate reader (SpectraMax® M2 System, Molecular Devices, UK). The control was performed with the cells cultured with medium without any treatment. Four independent experiments were conducted for CPP–P54 and three independent experiments for CPP–P54/PEG–P54, each with triplicate samples. The half maximal inhibitory concentration (IC_{50}) was determined from the dose–response curve. No toxic effect was observed for free peptides.

In vivo experiments

Animals. Female nude mice Rj: NMRI-Foxn1 nu/nu of 7 weeks (JANVIER LABS, Saint Berthevin, France) were housed in the Angers University Hospital animal facility. They were provided with food and water and followed a regular 12 hour day/night cycle. After a week of acclimatization, the animals were used for percutaneous intrapulmonary lung cell cancer administration and intratracheal administration. Animal experiments were performed according to the ethics and regulation of animal experimentation: authorization no. 201805281630885.

Preparation of cell suspension and Matrigel® solution for injection. Matrigel® is a basement membrane matrix preparation extracted from Engelbreth–Holm–Swarm mouse sarcoma (ECM gel from Engelbreth–Holm–Swarm murine sarcoma, Sigma, E6909). It was mixed with the cell suspension in order to improve its attachment to the lung tissue and favor the formation of a mass. The received product was stocked at −80 °C and placed at 4 °C for 24 hours before its use. The received Matrigel® solution (with an initial concentration of 8–12 mg of protein per mL) was diluted 1/3 v/v in HBSS using calcium and magnesium before mixing with the cells. The human lung cancer cell line NCI-H460 was chosen to induce primary human lung cancer in nude mice. The cells received at least two passages between thawing and injection (the same media and multiplication time mentioned before were used). 24 h before the injection of the tumor cells, the Matrigel® and HBSS were stored at 4 °C and the Eppendorf tubes, the tips of pipettes and the syringes were stored at −20 °C in order to avoid any Matrigel® gelification before the injection. On the day of injection, 35 μL of 10^6 NCI-H460 cells in HBSS with calcium and magnesium was mixed with 35 μL of a solution of Matrigel® diluted as previously described in cold HBSS with calcium and magnesium. Mixing was performed in an ice bath at 4 °C so to keep the Matrigel® in a liquid form. The mice

were anesthetized by a continuous air flow (0.5–0.8 L min^{-1}) and using 20% isoflurane placed on their ventral side on a heating support to preserve their corporal temperature. The prepared cell suspension was slowly injected (7–10 seconds to inject 70 μL in order to allow the gelification of the Matrigel® inside the lungs) percutaneously using a syringe[29] into the left lateral thorax 3 mm above the line separating the lungs from the liver. The needle was inserted 4 mm into the thorax and quickly removed after the injection. Once the injection done, the mouse was woken up from the anaesthesia and observed until total recovery. The weight of the mice and their behavior, respiratory rate and response to normal stimulus were regularly checked.

MRI analyses. 9 days after the injection of cancerous cells, magnetic resonance imaging (MRI) was performed to identify the presence of lung tumors in the mice (Fig. S13†). MRI was performed using a PRISM core facility 7T scanner (Biospec 70/20 Avance III, Bruker Wissembourg, France) equipped with a BGA12S gradient system (675 mT m^{-1}) and a 35 mm diameter resonator. For the duration of all experiments under isoflurane anaesthesia, the animal temperature was regulated using a heated water-circulating system. After a set of localizing images, retrospectively gated T_1-weighted images were acquired to measure the volume of tumors using an IntraGate® FLASH 3D sequence (TR = 110 ms; TE = 1.6 ms; α = 50°; FOV = 25 × 25 mm; matrix = 192 × 192; nine slices of 0.7 mm).

Intratracheal administration. The mice with lung tumors were homogenously distributed into four groups, with three treated by nebulization of 3 different self-assemblies: Arg_9–P54/PEG–P54 (10/1 molar ratio), Arg_9–P54 and PEG–P54 at a concentration of 1 mM in P54 and a control group nebulized with physiological water. Two nebulization experiments have been performed at day 9 and day 12 after the injection of the tumor cells *via* the intratracheal route.[30] In order to regulate their osmolarity before nebulization, an adequate volume of a 9% NaCl solution was added to the different formulations. A final osmolarity of 280–300 mOsm L^{-1} was considered as suitable for a pulmonary administration.[53]

The mice were anesthetized by a continuous air flow (0.5–0.8 L min^{-1}) and using 2% isoflurane. The mice were fixed on an inclined support; it allowed visualizing the trachea of the mouse once its mouth is opened and the tongue is moved away from the field of vision. A laryngoscope was used to open the animal mouth and to take the tongue out of the way of vision. Once the trachea is clear, the syringe was introduced between the two vocal cords and the injection was performed.

In order to create an aerosol and mimic the nebulizer, a micro-sprayer system was used (high pressure syringe), allowing to create microdrops of the suspension, dispersing into the two lungs *via* an aerosol. The volume nebulized was of 50 μL. When the nebulization is over, the animal was waked up on a heating support and its behavior was carefully controlled until perfect recovery. Finally, the tumor size evolution was analyzed by MRI at different days: day 9, 12, 15, 21, 23, 25 and 27 after the injection of the tumor cells.

Mathematical modelling. First, the tumor volumes were measured from the MRI images. They were calculated from manually drawn ROI on each slice and the area being then multiplied by the slice thickness. These tumor volume growth curves were then fitted by the method of least squares with an exponential function and the time constant of exponential converted into a doubling time value as follows:[51] $V(t) = V_0 e^{\alpha t}$, where $V_0$is the volume at $t_0$and α the growth rate. If $V'(t') = V_0 e^{\alpha t'}$, t′ being chosen as V' = 2 V then $V_0 e^{\alpha t'} = 2V_0 e^{\alpha t}$, so $(t - t') = \ln(2)/\alpha$. $(t - t')$ being the doubling time.

Statistical analyses. In order to check if the data follow a normal law, two tests were performed: the Shapiro–Wilk test and the Kolmogorov–Smirnov test. Then a t test, with the correction of Welch, was performed to compare each treated group to the control group. Differences were considered as significant if the p value was <0.05.

Author contributions

L. Guyon has performed the synthesis, formulation and characterization parts with P54. She has written the first draft of the manuscript. A. Ladaycia has performed all the experiments with P819 and all the animal experiments. He has completed the first draft of the manuscript. A. Bosio has performed some *in vitro* experiments. L. Lemaire has performed the MRI experiments with A. Ladaycia. F. Franconi has performed the DOSY experiments and optimized the MRI protocol. B. Lelièvre has performed the preliminary ICP-MS experiments. N. Lautram has developed with L. Guyon and A. Ladaycia all the chromatographic methods. P. Pigeon has synthesized all the ferrocifens. G. Jaouen has supervised the ferrocifen synthesis. C. Passirani has supervised research. E. Lepeltier has analyzed the data, supervised research and designed the study. She has written the last version of the manuscript. The manuscript was written/revised through contributions of all authors. All authors have given approval to the final version of the manuscript.

Live subject statement

All animal procedures were performed in accordance with the Guidelines for Care and Use of Laboratory Animals of Angers University and approved by the Animal Ethics Committee of Angers authorization no. 201805281630885.

Data availability

The data supporting this article have been included as part of the ESI.† Additional raw data required to reproduce these findings can be made available upon request to the author.

Conflicts of interest

The authors declare no competing financial interest.

Acknowledgements

The authors would like to thank the support of the National Association of Research Technology (ANRt) *via* financing the PhD contract no.2016/68 and 2018/1485. The authors would like to thank Feroscan for its support. The authors would like to thank Benjamin Siegler for the DOSY experiments (Astral core facility, SFR Matrix, Univ Angers, France). The authors would like to acknowledge the PRISM core facility (Rennes-Angers, France) for support in the MRI experiments. Finally, the authors would like to thank Aurélien DuPont from the Microscopy Rennes Imaging Center for the Cryo-TEM images.

References

1 R. L. Siegel, K. D. Miller and A. Jemal, Cancer statistics, 2018, *CA Cancer J. Clin.*, 2018, **68**(1), 7–30.
2 C. Zappa and S. A. Mousa, Non-small cell lung cancer: current treatment and future advances, *Transl. Lung Cancer Res.*, 2016, **5**(3), 288–300.
3 A. Spira and D. S. Ettinger, Multidisciplinary management of lung cancer, *N. Engl. J. Med.*, 2004, **350**(4), 379–392.
4 D. Mahalingam, A. Mita, M. M. Mita, S. T. Nawrocki and F. J. Giles, Targeted therapy for advanced non-small cell lung cancers: historical perspective, current practices, and future development, *Curr. Probl. Cancer*, 2009, **33**(2), 73–111.
5 C. Y. Huang, D. T. Ju, C. F. Chang, P. Muralidhar Reddy and B. K. Velmurugan, A review on the effects of current chemotherapy drugs and natural agents in treating non-small cell lung cancer, *Biomedicine*, 2017, **7**(4), 23.
6 L. Guyon, E. Lepeltier and C. Passirani, Self-assembly of peptide-based nanostructures: Synthesis and biological activity, *Nano Res.*, 2018, **11**(5), 2315–2335.
7 L. Guyon, E. Lepeltier, J. C. Gimel, B. Calvignac, F. Franconi, N. Lautram, *et al.*, Importance of Combining Advanced Particle Size Analysis Techniques To Characterize Cell-Penetrating Peptide–Ferrocifen Self-Assemblies, *J. Phys. Chem. Lett.*, 2019, **10**(21), 6613–6620.
8 E. Lepeltier, L. Guyon, A. Ladaycia, G. Jaouen and C. Passirani, Self-assemblies of ferrocifen conjugates for lung cancer treatment, *European Patent* EP223055591, 2022.
9 C. Bechara and S. Sagan, Cell-penetrating peptides: 20 years later, where do we stand?, *FEBS Lett.*, 2013, **587**(12), 1693–1702.
10 J. Xu, A. R. Khan, M. Fu, R. Wang, J. Ji and G. Zhai, Cell-penetrating peptide: a means of breaking through the physiological barriers of different tissues and organs, *J. Controlled Release*, 2019, **309**, 106–124.
11 M. Lindgren, M. Hällbrink, A. Prochiantz and U. Langel, Cell-penetrating peptides, *Trends Pharmacol. Sci.*, 2000, **21**(3), 99–103.
12 J. D. Hartgerink, E. Beniash and S. I. Stupp, Peptide-amphiphile nanofibers A versatile scaffold for the preparation of self- assembling materials, *Proc. Natl. Acad. Sci. USA*, 2002, **99**, 5133–5138.
13 S. Soukasene, D. J. Toft, T. J. Moyer, H. Lu, H. K. Lee, S. M. Standley, *et al.*, Antitumor activity of peptide amphiphile nanofiber-encapsulated camptothecin, *ACS Nano*, 2011, **5**(11), 9113–9121.
14 R. Lin, A. G. Cheetham, P. Zhang, Y. Lin and H. Cui, Supramolecular filaments containing a fixed 41% paclitaxel loading, *Chem. Commun.*, 2013, **49**(43), 4968–4970.
15 G. Jaouen, A. Vessieres and S. Top, Ferrocifen type anti cancer drugs, *Chem. Soc. Rev.*, 2015, **44**(24), 8802–8817.
16 G. Jaouen and S. Top, The Ferrocifen Family as Potent and Selective Antitumor Compounds: Mechanisms of Action, in *Advances in Organometallic Chemistry and Catalysis*, John Wiley & Sons, Ltd, 2013, pp. 563–580. Disponible sur: **https://online-library.wiley.com/doi/abs/10.1002/9781118742952.ch42**.
17 S. Top, A. Vessières, G. Leclercq, J. Quivy, J. Tang, J. Vaissermann, *et al.*, Synthesis, biochemical properties and molecular modelling studies of organometallic specific estrogen receptor modulators (SERMs), the ferrocifens and hydroxyferrocifens: evidence for an antiproliferative effect of hydroxyferrocifens on both hormone-dependent and hormone-independent breast cancer cell lines, *Chemistry*, 2003, **9**(21), 5223–5236.
18 W. Yang, Y. Xia, Y. Fang, F. Meng, J. Zhang, R. Cheng, *et al.*, Selective Cell Penetrating Peptide-Functionalized Polymersomes Mediate Efficient and Targeted Delivery of Methotrexate Disodium to Human Lung Cancer In Vivo, *Adv. Healthc. Mater.*, 2018, **7**(7), e1701135.
19 E. Kondo, K. Saito, Y. Tashiro, K. Kamide, S. Uno, T. Furuya, *et al.*, Tumour lineage-homing cell-penetrating peptides as anticancer molecular delivery systems, *Nat. Commun.*, 2012, **3**, 951.
20 H. Gao, Q. Zhang, Y. Yang, X. Jiang and Q. He, Tumor homing cell penetrating peptide decorated nanoparticles used for enhancing tumor targeting delivery and therapy, *Int. J. Pharm.*, 2015, **478**(1), 240–250.
21 S. Futaki, T. Suzuki, W. Ohashi, T. Yagami, S. Tanaka, K. Ueda, *et al.*, Arginine-rich peptides. An abundant source of membrane-permeable peptides having potential as carriers for intracellular protein delivery, *J. Biol. Chem.*, 2001, **276**(8), 5836–5840.
22 D. J. Mitchell, D. T. Kim, L. Steinman, C. G. Fathman and J. B. Rothbard, Polyarginine enters cells more efficiently than other polycationic homopolymers, *J. Pept. Res.*, 2000, **56**(5), 318–325.
23 R. Rosière, J. Hureaux, V. Levet, K. Amighi and N. Wauthoz, La chimiothérapie inhalée – partie 1: concept et challenges technologiques actuels, *Rev. Mal. Respir.*, 2018, **35**(4), 357–377.
24 R. Rosière, J. Hureaux, V. Levet, K. Amighi and N. Wauthoz, La chimiothérapie inhalée – partie 2: clinique et applications potentielles, *Rev. Mal. Respir.*, 2018, **35**(4), 378–389.

25 S. K. Lai, D. E. O'Hanlon, S. Harrold, S. T. Man, Y. Y. Wang, R. Cone, *et al.*, Rapid transport of large polymeric nanoparticles in fresh undiluted human mucus, *Proc. Natl. Acad. Sci. U. S. A.*, 2007, **104**(5), 1482–1487.
26 Y. Y. Wang, S. K. Lai, J. S. Suk, A. Pace, R. Cone and J. Hanes, Addressing the PEG mucoadhesivity paradox to engineer nanoparticles that "slip" through the human mucus barrier, *Angew. Chem., Int. Ed.*, 2008, **47**(50), 9726–9729.
27 M. Yang, S. K. Lai, Y. Y. Wang, W. Zhong, C. Happe, M. Zhang, *et al.*, Biodegradable nanoparticles composed entirely of safe materials that rapidly penetrate human mucus, *Angew. Chem., Int. Ed.*, 2011, **50**(11), 2597–2600.
28 J. T. Huckaby and S. K. Lai, PEGylation for enhancing nanoparticle diffusion in mucus, *Adv. Drug Delivery Rev.*, 2018, **124**, 125–139.
29 J. Hureaux and T. Urban, Mise au point d'un modèle de cancer bronchique orthotopique chez la souris, *Rev. Mal. Respir.*, 2015, **32**, A96.
30 J. Hureaux, F. Lacoeuille, F. Lagarce, M. C. Rousselet, A. Contini, P. Saulnier, *et al.*, Absence of lung fibrosis after a single pulmonary delivery of lipid nanocapsules in rats, *Int. J. Nanomed.*, 2017, **12**, 8159–8170.
31 M. Bivas-Benita, R. Zwier, H. E. Junginger and G. Borchard, Non-invasive pulmonary aerosol delivery in mice by the endotracheal route, *Eur. J. Pharm. Biopharm.*, 2005, **61**(3), 214–218.
32 F. Gagnadoux, A. Le Pape, T. Urban, J. Montharu, L. Vecellio, J. C. Dubus, *et al.*, Safety of pulmonary administration of gemcitabine in rats, *J. Aerosol Med.*, 2005, **18**(2), 198–206.
33 P. Pigeon, Y. Wang, S. Top, F. Najlaoui, M. C. Garcia Alvarez, J. Bignon, *et al.*, A New Series of Succinimido-ferrociphenols and Related Heterocyclic Species Induce Strong Antiproliferative Effects, Especially against Ovarian Cancer Cells Resistant to Cisplatin, *J. Med. Chem.*, 2017, **60**(20), 8358–8368.
34 Y. Wang, P. Pigeon, W. Li, J. Yan, P. M. Dansette, M. Othman, *et al.*, Diversity-oriented synthesis and bioactivity evaluation of N-substituted ferrocifen compounds as novel antiproliferative agents against TNBC cancer cells, *Eur. J. Med. Chem.*, 2022, **234**, 114202.
35 V. Glushko, M. S. Thaler and C. D. Karp, Pyrene fluorescence fine structure as a polarity probe of hydrophobic regions: behavior in model solvents, *Arch. Biochem. Biophys.*, 1981, **210**(1), 33–42.
36 A. S. Patha, T. Patil, P. K. Pandey, K. Kuche, R. Ghadi and S. Jain, Chapter 7 - Block copolymer micelles as long-circulating drug vehicles, in *Smart Polymeric Nano-Constructs in Drug Delivery*, ed. S. P. Vyas, U. Agrawal and R. Sharma, Academic Press, 2023, pp. 187–220. Disponible sur: **https://www.sciencedirect.com/science/article/pii/B9780323912488000088**.
37 F. Franconi, L. Lemaire, J. C. Gimel, S. Bonnet and P. Saulnier, NMR diffusometry: A new perspective for nanomedicine exploration, *J. Controlled Release*, 2021, **337**, 155–167.
38 A. Bernkop-Schnürch, Strategies to overcome the polycation dilemma in drug delivery, *Adv. Drug Delivery Rev.*, 2018, **136–137**, 62–72.
39 E. Koren, A. Apte, R. R. Sawant, J. Grunwald and V. P. Torchilin, Cell-penetrating TAT peptide in drug delivery systems: proteolytic stability requirements, *Drug Delivery*, 2011, **18**(5), 377–384.
40 A. Henning, M. Schneider, N. Nafee, L. Muijs, E. Rytting, X. Wang, *et al.*, Influence of particle size and material properties on mucociliary clearance from the airways, *J. Aerosol Med. Pulm. Drug Delivery*, 2010, **23**(4), 233–241.
41 L. Sanchez, Y. Yi and Y. Yu, Effect of partial PEGylation on particle uptake by macrophages, *Nanoscale*, 2017, **9**(1), 288–297.
42 Q. Xu, L. M. Ensign, N. J. Boylan, A. Schön, X. Gong, J. C. Yang, *et al.*, Impact of Surface Polyethylene Glycol (PEG) Density on Biodegradable Nanoparticle Transport in Mucus ex Vivo and Distribution in Vivo, *ACS Nano*, 2015, **9**(9), 9217–9227.
43 V. Scalcon, R. Bonsignore, J. Aupič, S. R. Thomas, A. Folda, A. A. Heidecker, *et al.*, Exploring the Anticancer Activity of Tamoxifen-Based Metal Complexes Targeting Mitochondria, *J. Med. Chem.*, 2023, **66**(14), 9823–9841.
44 S. A. Bode and D. W. P. M. Löwik, Constrained cell penetrating peptides, *Drug Discovery Today: Technol.*, 2017, **26**, 33–42.
45 L. Zhu, P. Kate and V. P. Torchilin, Matrix metalloprotease 2-responsive multifunctional liposomal nanocarrier for enhanced tumor targeting, *ACS Nano*, 2012, **6**(4), 3491–3498.
46 L. Zhu, T. Wang, F. Perche, A. Taigind and V. P. Torchilin, Enhanced anticancer activity of nanopreparation containing an MMP2-sensitive PEG-drug conjugate and cell-penetrating moiety, *Proc. Natl. Acad. Sci. U. S. A.*, 2013, **110**(42), 17047–17052.
47 Q. Yang, S. W. Jones, C. L. Parker, W. C. Zamboni, J. E. Bear and S. K. Lai, Evading immune cell uptake and clearance requires PEG grafting at densities substantially exceeding the minimum for brush conformation, *Mol. Pharm.*, 2014, **11**(4), 1250–1258.
48 B. Pelaz, P. del Pino, P. Maffre, R. Hartmann, M. Gallego, S. Rivera-Fernández, *et al.*, Surface Functionalization of Nanoparticles with Polyethylene Glycol: Effects on Protein Adsorption and Cellular Uptake, *ACS Nano*, 2015, **9**(7), 6996–7008.
49 D. Pozzi, V. Colapicchioni, G. Caracciolo, S. Piovesana, A. L. Capriotti, S. Palchetti, *et al.*, Effect of polyethyleneglycol (PEG) chain length on the bio–nano-interactions between PEGylated lipid nanoparticles and biological fluids: from nanostructure to uptake in cancer cells, *Nanoscale*, 2014, **6**(5), 2782–2792.
50 T. A. Aguilera, E. S. Olson, M. M. Timmers, T. Jiang and R. Y. Tsien, Systemic in vivo distribution of activatable cell penetrating peptides is superior to that of cell penetrating peptides, *Integr. Biol.*, 2009, **1**(5–6), 371–381.
51 L. Lemaire, F. Franconi, B. Siegler, C. Legendre and E. Garcion, In vitro expansion of U87-MG human glioblastoma cells under

hypoxic conditions affects glucose metabolism and subsequent in vivo growth, *Tumour Biol.*, 2015, **36**(10), 7699–7710.
52 Q. Fan, Y. Ji, J. Wang, L. Wu, W. Li, R. Chen, *et al.*, Self-assembly behaviours of peptide–drug conjugates: influence of multiple factors on aggregate morphology and potential self-assembly mechanism, *R. Soc. Open Sci.*, 2018, **5**(4), 172040.
53 G. Pilcer and K. Amighi, Formulation strategy and use of excipients in pulmonary drug delivery, *Int. J. Pharm.*, 2010, **392**(1), 1–19.